"Activated Borane" – A Porous Borane Cluster Network

Daniel Bůžek,[a,b] Karel Škoch,[a] Soňa Ondrušová,[a] Matouš Kloda,[a] Dmytro Bavol,[a] Andrii Mahun,[c] Libor Kobera,[c] Kamil Lang,[a] Michael G. S. Londesborough,[a] Jan Demel[a*]*
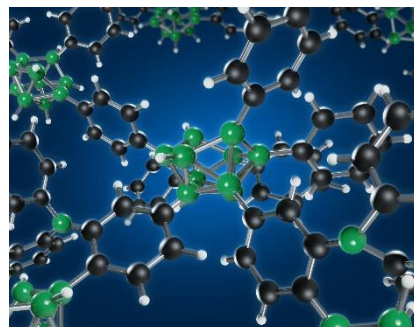
[a] Institute of Inorganic Chemistry of the Czech Academy of Sciences, 250 68 Řež, Czech Republic; E-mail: demel@iic.cas.cz

[b] Faculty of Environment, Jan Evangelista Purkyně University, Pasteurova 3632/15, 400 96 Ústí nad Labem, Czech Republic

[c] Institute of Macromolecular Chemistry of the Czech Academy of Sciences, Heyrovského nám. 2, 162 06, Prague 6, Czech Republic

TOC

Porous polymer: Thermolysis of *nido*-$B_{10}H_{14}$ and toluene at 250°C affords the novel microporous polymer named "*Activated Borane*". Analyses suggests an amorphous structure of borane clusters interconnected by toluene moieties. *Activated Borane* displays a high surface area of 774 m^2g^{-1}, thermal stability under Ar up to 1000°C, and sorption capacity to emerging pollutants exceeding the capacity of commercial *activated carbon*.

Abstract:

The unprecedented co-thermolysis of *nido*-decaborane ($B_{10}H_{14}$) and toluene results in a novel porous material (that we have named "*Activated Borane*") containing micropores of 1.0 and 1.5 nm in diameter and a specific surface area of 774 $m^2\,g^{-1}$ (Ar, 87 K) that is thermally stable up to 1000 °C. Solid-state ^1H, ^{11}B and ^{13}C MAS NMR, UV-vis and IR spectroscopies suggest an

1

amorphous structure of borane clusters interconnected by toluene moieties in a ratio of about three toluene molecules for every borane cluster. In addition, the structure contains Lewis-acidic tri-coordinated boron sites giving it some unique properties. *Activated Borane* displays high sorption capacity for pollutants such as sulfamethoxazole, tramadol, diclofenac and bisphenol A that exceed the capacity of commercially-available *activated carbon*. The consistency in properties for each batch made, and the ease of its synthesis, make *Activated Borane* a promising porous material worthy of broad attention.

Introduction

Porous materials are highly versatile and are used in a growing range of applications including adsorption processes (e.g., gas storage and separation, pollutant removal), heterogeneous catalysis, drug delivery, energy storage, etc.[1] An ultimate goal in the development of porous materials is to tailor the size, shape and connectivity of pores and their chemical nature to suit specific applications, while keeping the synthetic process simple and cost effective.

The chemical nature of porous materials is diverse, it comprises (i) Organic polymers such as porous carbons (thermally, chemically or physically activated organic precursors),[2] hyper-crosslinked porous polymers (Davankov resins),[3] covalent organic frameworks (COFs),[4] polymers of intrinsic microporosity (PIMs),[5] etc. In these cases, the "backbone" of the polymer consists of bonds created from the organic chemistry toolbox (e.g., C-C bond, C-N bond, boroxine, etc.). (ii) Inorganic materials such as zeolites,[6] aluminophosphates,[7] mesoporous molecular sieves,[8] porous titania,[9] etc. are based on 3-dimensional networks of bridging oxygen atoms and Si, Al, Ti as well as other metals or semi-metals. (iii) Porous coordination polymers (Metal-organic frameworks, MOFs)[10] are based on arrays of metal atoms or oxometalate clusters bound together by organic ligands through coordination bonds.

Each of the above classes possess different properties, suitable for specific applications, made possible by the chemical and structural diversity amongst individual materials. For this reason, it is highly desirable to further widen the portfolio of porous materials by seeking new avenues to their construction. In this context, there is a gap in the literature when it comes to porous materials based on borane clusters (boranes) connected directly by B-B bond or by short alkyl or aryl bridges – B-C bonds.

2

Boron has one valence electron fewer than its number of valence orbitals, resulting in an electron deficiency that leads the hydrides of boron to share electron density in spherically-aromatic delocalized manners. This results in some unique structural motifs and properties that are hard to find in the chemistry of other elements, these include (i) reverse $B^{\delta+}$-$H^{\delta-}$ polarity, (ii) 3D spherically aromatic character, (iii) thermal stability and low toxicity of closed borane cages due to high resistance to biological degradation.[11,12,13,14]

In this paper we present a new strategy for the synthesis of porous polymers by simple heating of decaborane(14) (*nido*-$B_{10}H_{14}$) in toluene. We named the resulting porous polymer *Activated Borane* (**ActB**) due to the similarity of its synthetic procedure and simplicity of preparation with *Activated Carbon*.[2] We provide initial characterization data that suggest a structure of borane clusters connected by tolyl bridges, and showcase the exciting potential of this new group of porous polymers as adsorbents of emerging pollutants, such as the antibiotic sulfamethoxazol, in which **ActB** displays 50% higher sorption capacity of than *Activated Carbon* (Sigma-Aldrich).

Results and discussion

Synthesis of Activated Borane

ActB was prepared by heating a mixture of *nido*-$B_{10}H_{14}$ in toluene to 250 °C for 24 h. The reaction was conducted in a sealed glass ampoule inserted into an autoclave containing toluene as a medium to compensate for the high pressure developed within the ampoule. Special attention was taken when opening the ampoule, which is necessary to cool to 77 K in order to reduce the pressure inside. The resulting black mixture was Soxhlet extracted for 2 days with toluene. Removal of residual solvent (activation) was done by heating to 100 °C under dynamic vacuum. For experimental details see ESI.
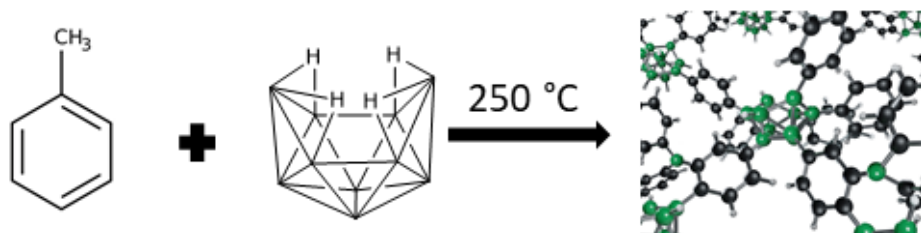
Figure 1. Schematic representation of the reaction forming **ActB**.

ActB can be synthetized readily from commercially available materials without any purification; however, best results are achieved when **ActB** is synthetized in the absence of moisture and air (for details see below) using standard Schlenk techniques and Ar-filled glovebox.

Characterization

ActB displays a type I adsorption isotherm of argon typical for microporous materials (see Figure 2, top right) and has a BET (Brunauer, Emmett and Teller) specific surface area (S_{BET}) of 774 ± 35 m^2g^{-1}. The batch-to-batch reproducibility for this parameter is very good, with S_{BET} differences between batches being within experimental error of the method (<5 %, for details see Table S1). The calculated pore size distribution (Figure S1) gives two rather sharp maxima centred around 1.0 nm and 1.5 nm. This distribution is rather unusual for amorphous polymers, which generally display either a broad distribution of pores or pores larger than 2 nm (mesopores). The fact that the pores are reproducibly of the same size indicates that even though **ActB** has no short-range order there is a regularity at the nanometric level and manifests in the relatively uniform manner of its
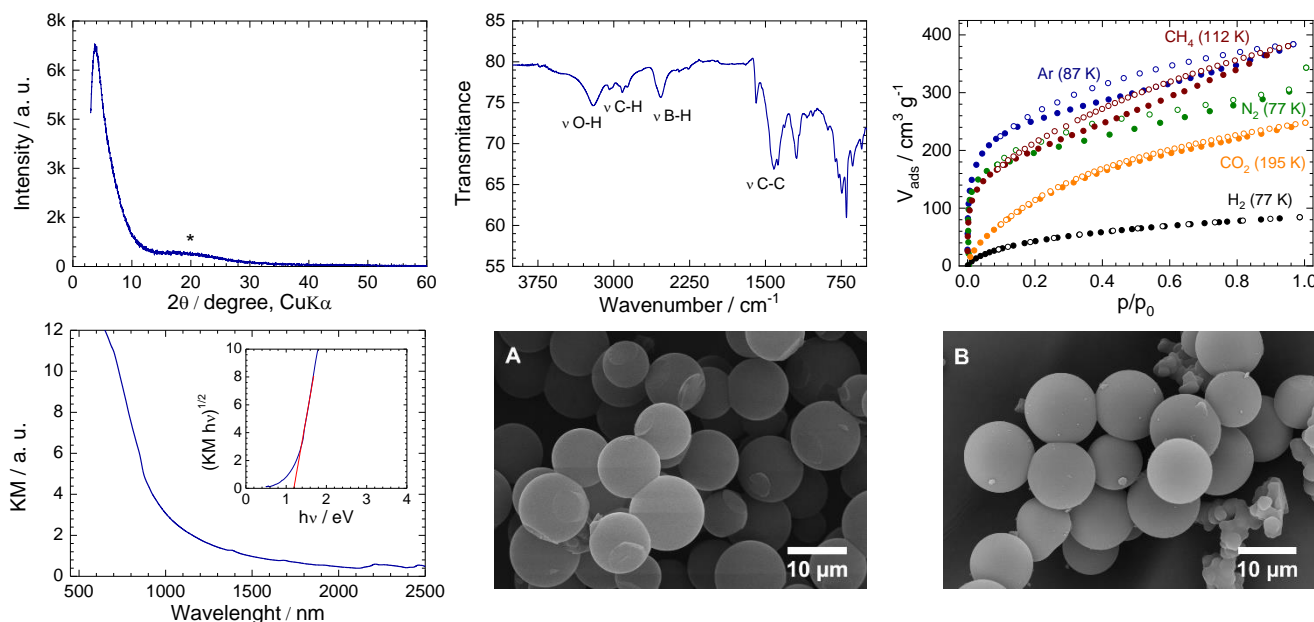
Figure 2. From top left: Powder X-ray diffraction pattern of **ActB** (* represents the diffraction of sample holder); FTIR spectrum of **ActB**; Adsorption isotherms of **ActB**. Bottom row from left: UV-vis spectrum of **ActB** with Kubelka−Munk-transformed reflectance spectra in the inset; SEM images of two different batches of **ActB**.

pore sizes. Figure 2 shows a comparison of adsorption isotherms of Ar, N_2, CO_2 and CH_4 measured at temperatures of their respective boiling points and H_2 measured at 77 K. As can be seen, methane and argon adsorb into the micropores of **ActB** in a similar manner, whereas the volume of adsorbed CO_2 is significantly lower.

Unfortunately, the structural analysis is not straight forward; **ActB** displays only one broad peak, at around 27 Å, in the powder X-ray diffraction pattern (Figure 2 top left). This suggests only a very low degree of ordering. Elemental analysis (Table S2) determined the C, B and H molar ratio as ca. 2 : 1 : 2.5, respectively, which corresponds to three molecules of toluene to every decaborane cluster with a high degree of cross-linking.

The FTIR spectrum (Figure 2 top middle) of **ActB** display vibrations from both entities – borane cluster, mainly B-H vibrations, and from toluene – mainly stretching vibrations of aromatic and aliphatic C-H bonds and C-C bonds. Additionally, the peak at approximately 3200 cm^{-1} can be ascribed to the vibrations of BO-H bonds. This adds weight to the probability that borane clusters are preserved in the structure, however, despite all efforts to exclude air and moisture from the synthesis, some oxygen contamination is present, possibly originating from reaction with the walls

of the glass ampoule. Indeed, such reactivity between borane clusters and glass surfaces has been noted previously during high-energy UV experiments on organic solutions of the related borane *anti*-$B_{18}H_{22}$.[15,16] The absence of peak at around 1900 cm^{-1} indicates that **ActB** does not contain significant number of μ-H (B-H-B bridges) that are located at the open face of *nido* and *arachno* borane clusters. This observation is in good agreement with our findings from solid state NMR spectroscopic measurements described below.

The UV-vis spectrum of **ActB** (Figure 2 bottom left) shows strong absorption below 1000 nm, this translates to an optical band gap of 1.19 eV derived from the Kubelka−Munk-transformed reflectance spectra. Additionally, **ActB** displays weak luminescence upon excitation at 500 nm with a broad maximum at approximately 750 nm (see Figure S3).

Scanning electron microscopy (SEM) shows spherical particles with diameters of approximately 10 µm. The number of smaller spheres and non-spherical particles varied from batch to batch. The thermogravimetric analysis (TGA) performed in Ar atmosphere documents high thermal stability up to 1000°C (see Figure 3). The majority of the approximately 11 % decrease in mass between RT and 1000 °C can be attributed to the loss of toluene with the maximum at around 300 °C. This feature bodes well for possible application where high temperature is a prerequisite.
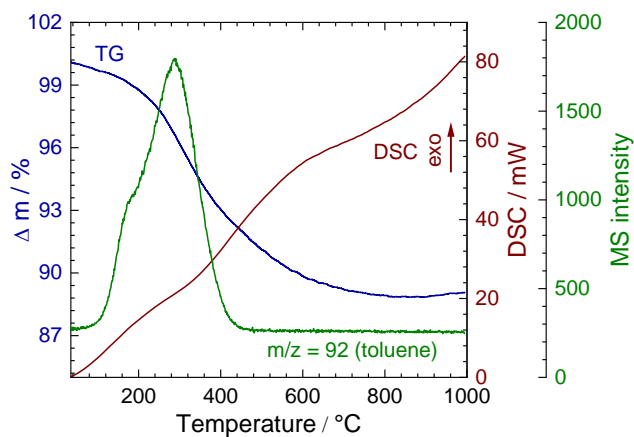

Figure 3. Thermogravimetric analysis of **ActB** performed in Ar atmosphere. Blue is thermogravimetric curve, red curve differential scanning calorimetry (DSC) and green curve signal from mass spectrometry for toluene (m/z = 92).

ActB is insoluble in all common non-polar solvents and only negligible amount can be dissolved in polar solvents, such as THF. For this reason, the structure of **ActB** was probed using ^{1}H, ^{11}B and ^{13}C solid state NMR (ssNMR) analyses and compared with parent *nido*-$B_{10}H_{14}$ and literature data, see Figure 4.[17] The ^{1}H magic angle spinning (MAS) NMR spectrum of **ActB** (Figure 4b) displays two broad and almost unresolved signals with chemical shifts 1.95 and 6.55 ppm. They can be attributed to methylene groups and aromatic hydrogen atoms from toluene with a contribution from *nido*-$B_{10}H_{14}$ hydrogen atoms. Interestingly, bridging hydrogen atoms (μ marked in Figure 4a) are missing in **ActB**. To confirm this, we measured ^{1}H high resolution-NMR experiment of **ActB** suspended in dried d_8-THF, see Figure S5. In this configuration part of the borane species dissolved confirming the absence of boranes containing μ hydrogens (usually seen in the 0 to -4 ppm range). Reasonable explanations for these observations are the transformation of open *nido*-borane clusters to closed *closo*-borane clusters and/or full substitution of μ hydrogen atoms.

The ^{11}B MAS NMR spectrum of **ActB** is an accumulation of overlapping resonances to give one broad asymmetric peak with a maximum at -8.3 ppm. As such, the amount of information discernible from this NMR technique is limited. Nevertheless, what is clear from the ^{11}B spectrum of **ActB** (Figure 4, a) compared to that of *nido*-$B_{10}H_{14}$ (Figure 4, b) is the downfield shift of the peak for boron atoms B2 and B4, and, conversely, the upfield shifts in the resonances for the remaining boron atoms in the cluster species. This shifting in magnetic shielding and deshielding, suggests that the decaborane molecule is being substituted in multiple positions, causing marked fluctuations in its distribution of electron density within the cluster and consequent change in its ^{11}B NMR spectrum that is apparent in Figure 4. Additionally, a prominent shoulder at ca. 20 ppm (see dashed box in Figure 5b) indicates the presence of a tri-coordinated boron (B^{III}) species. This is supported by ^{11}B spin-echo MAS NMR and ^{11}B 3Q/MAS NMR spectra, see Figure 5, which indicate the presence of a B^{III} species with δ_{iso} = 20.3 ppm. Additional structural information was extracted from ^{11}B high resolution-NMR spectroscopy of an **ActB** sample suspended in dried d_8-THF, see Figure S5. These spectra confirmed the presence of B^{III} species and the comparison of {^{1}H} decoupled and undecoupled spectra clearly exclude that B^{III} species would be directly connected to hydrogen atoms. (In case of the existence of B-H bonds, a J^1(^{11}B-^{1}H) splitting would be visible in the undecoupled spectrum). Moreover, the minimal broadening of B^{III} signals in the two spectra in comparison to pure H_3BO_3 in D_2O indicates that the tri-coordinated boron species in the **ActB** sample is no longer a part of the borane clusters as that would lead to much broader

7

corresponding signals (see Figure S5). For this to happen, the B^{III} must have been expelled from the borane cluster, the mechanism of which is currently unclear. However, the formation of H_3BO_3 has been previously noted to form during anaerobic high-energy laser processes involving boranes in silica-glass vessels[15,16] and so the origin of the oxygen might be the glass ampoule. The extracted NMR parameters ($\delta_{iso} = 20.0$ ppm, $C_Q = 2.5$ MHz and $\eta = 0.17$) of the B^{III} species from ^{11}B MAS spin-echo NMR (8 loops) spectrum suggest formation of boronic acids/esters.[18,19] The presence of B^{III} species suggests that more complicated transformations are taking place during the synthesis, it is highly probable that some of the borane clusters may be merging and/or disassembling.
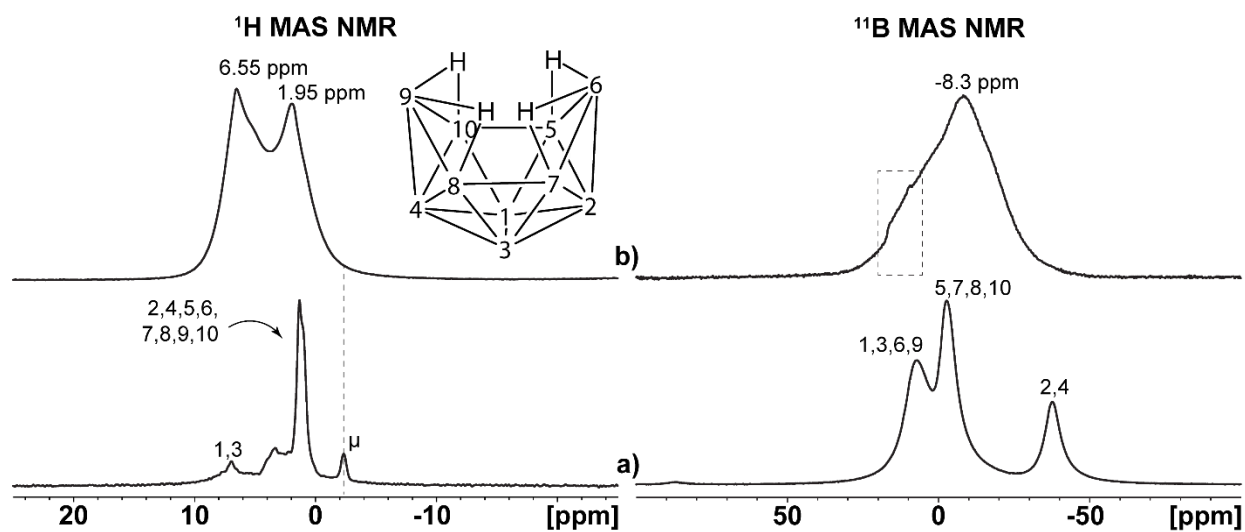

Figure 4. Measured ^1H MAS NMR (left-hand column) and ^{11}B MAS NMR (right-hand column) spectra of *nido*-decaborane a) and **ActB** b), respectively.
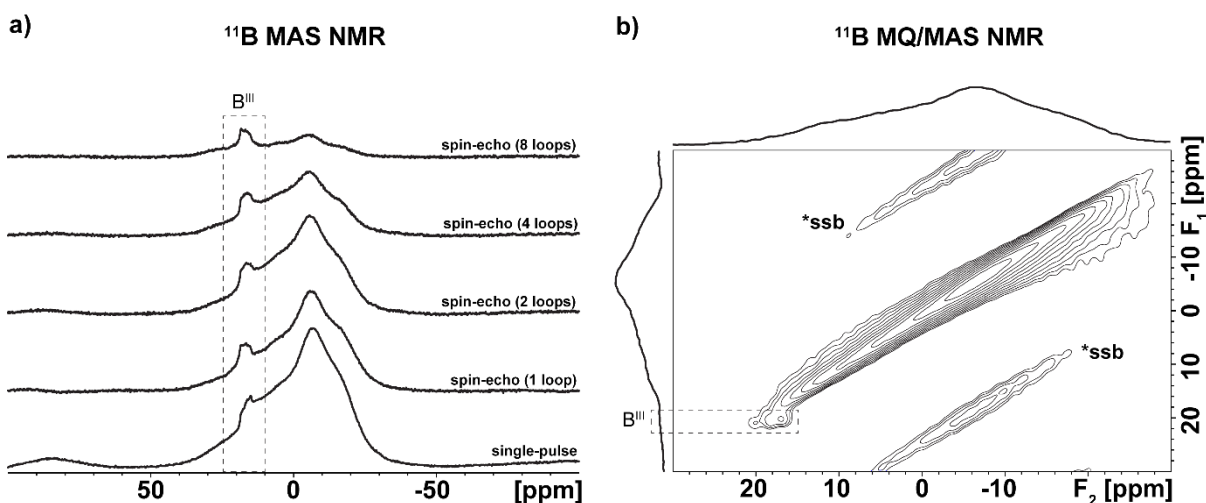
Figure 5. The ^{11}B spin-echo MAS NMR spectra a) and ^{11}B 3Q/MAS NMR spectrum b) of **ActB** sample acquired on 16.4 T NMR spectrometer at 20 kHz spinning speed of sample.

The ^{13}C MAS NMR spectra measured with and without cross polarization (CP) are near to identical (see Figure S6), which means that all carbon components in the structure are immobilized without significant rotation. The ^{13}C CP/MAS NMR spectrum (see Figure 6) contains three dominant and relatively narrow peaks (19.4 ppm, 126.7 ppm and 134.6 ppm) which are attributed to methylene groups (-CH$_3$) and two non-equivalent aromatic carbons (=CH-) from immobilized toluene, respectively. However, two additional signals; one relatively narrow peak at 0.5 ppm and a second broader peak at 29.3 ppm, were also detected (see Figure 6, dashed lines). The signal at 0.5 ppm can be attributed to carbon atoms bonded to borane clusters and form nodal points between borane clusters, similarly as known from boron carbide.[20,21] On the other hand, the broad signal at 29.3 ppm ranging from 70 ppm to -10 ppm can be attributed to methylene groups directly connected to borane clusters and/or carbons incorporated into these clusters possibly forming a substituted carborane cluster (C$_2$B$_{10}$H$_{12}$).[22]

Another information regarding the structure of **ActB** can be drawn from the study of thermolysis of *nido*-decaborane in aromatic solvents (manuscript under preparation). These findings show that there are at least two reactions taking place: substitution of decaborane with aromatic solvent molecules and fusion of decaborane clusters to form B$_{18}$H$_{22}$. The later reaction can be the source of tricoordinated boron species that was expelled from decaborane cluster during cluster fusion.
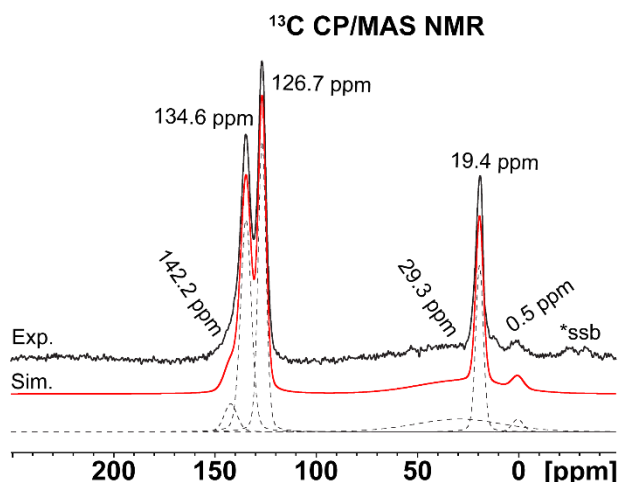
Figure 6. Experimental ^{13}C CP/MAS NMR spectra (black solid line), simulations of the individual carbon sites (dashed lines) and their sum (red solid line) of **ActB**. Spinning side band is denoted *ssb.

Properties

To investigate the properties of **ActB** and demonstrate its potential for application, we tested its adsorption and extraction of drug molecules from water. Pharmaceuticals are considered as contaminants of emerging concern (CEC) because of their widespread diffusion in surface waters and their recognized adverse effects on aquatic organisms. The chemical nature of many pharmaceuticals precludes their effective removal via typical waste or drinking water treatment processes, often resulting in their re-entry into the aquatic ecosystem.[23,24,25] For these reasons, European directives encourage the development of new strategies for reducing pharmaceuticals from waste waters, especially antibiotics.[26]

Thus, we selected the common antibiotic sulfamethoxazole as a model pollutant for adsorption experiments.[27] Adsorption kinetics (Figure 7) for **ActB** of sulfamethoxazole showed rapid adsorption of the pollutant during the first few minutes. The **ActB** adsorbent reached partial saturation after 60 min, however, **ActB** can accommodate further small amounts of the pollutant also after this time (adsorbed amount at 1 h and 24 h was 270 mg g^{-1} and 284 mg g^{-1}, respectively). Pseudo-second order model kinetics match the experimental data well (see fitted parameters at Table S2) indicating fast adsorption at the beginning, which is a key feature of any prospective adsorbent for environmental protection or emergency removal of the contaminants.

10

To test the stability of **ActB** in water we prolonged the shaking period of **ActB** in solution of sulfamethoxazole to 28 days and followed the concentration of sulfamethoxazole. As can be seen from Figure S7 we did not observe any degradation of **ActB** that would be related with desorption of sulfamethoxazole.

The middle graph of Figure 7 shows the adsorption isotherms (initial concentration ranged from 10 to 100 mg L^{-1}, samples taken after 24 h of shaking at 25$\pm$1 °C) of sulfamethoxazole onto **ActB** next to that for *activated carbon* (Sigma Aldrich) as a comparison. Both isotherms were fitted by Langmuir and Freundlich mathematical models of adsorption (for details including the fitting parameters and fitting curves see Figure S8 and Table S3 in ESI). From this data, it is clear that **ActB**, with an adsorption capacity of 325 mg g^{-1}, displays 50 % higher sorption capacity than *activated carbon* (219 mg g^{-1}) while the K_L parameters are similar for both adsorbents indicating that adsorbent-adsorbate affinities are comparable.

Motivated by these results, we tested further the effect of **ActB** on other hard to remove pollutants commonly occurring in waters – tramadol (tramadol hydrochloride, analgesic), diclofenac (diclofenac sodium salt, analgesics and anti-inflammatory drug) and bisphenol A (polymer component that acts in human body as endocrine disruptor). The graph on the right-hand side of Figure 7 shows the extent of removal of the pollutants (initial concentrations of 100 mg L^{-1}) after 24 h of shaking. Direct comparison with *activated carbon* again shows the superior sorption capacity of **ActB.** More specifically, **ActB** can accommodate 1.6x and 2.5x larger amounts of diclofenac and tramadol than *activated carbon*, respectively. One possible explanation for the higher affinity towards the aforementioned pharmaceuticals could be the interaction of Lewis-basic nitrogen atoms present in the pollutant molecules with the Lewis acidic tricoordinated boron sites in **ActB** that we describe above in the discussion of the ssNMR analyses. Despite the exact nature of these Lewis acidic centres remains unknown, their presence seems to impart some unique properties to **ActB**.
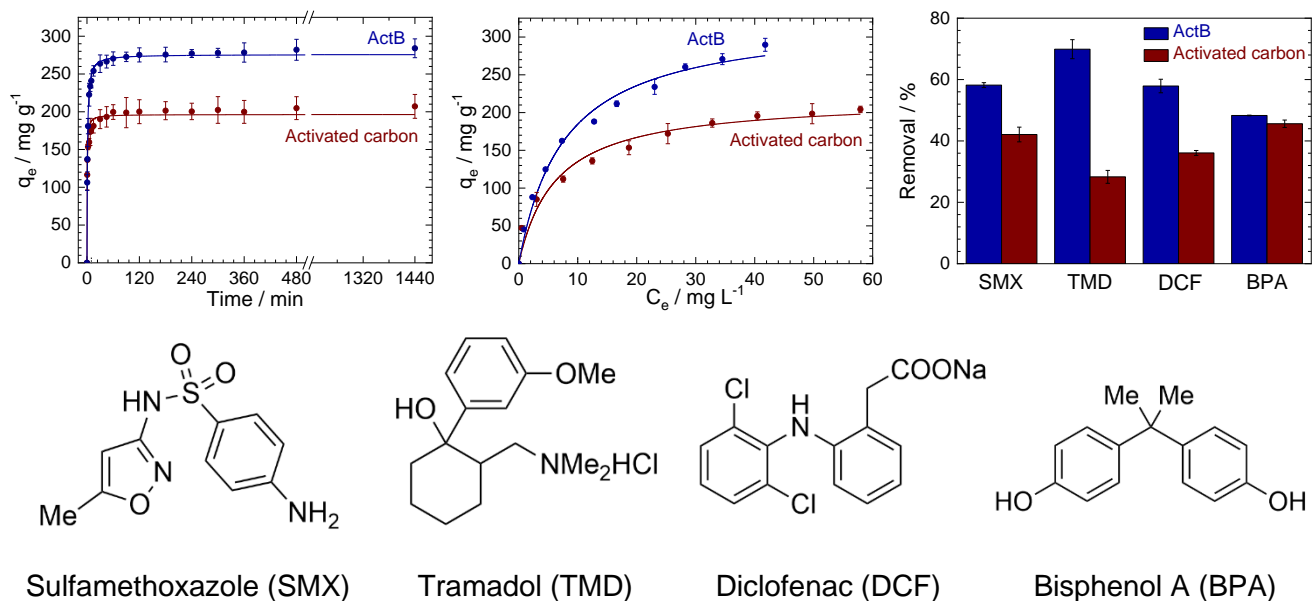
Figure 7. Adsorption of pollutants on **ActB** and its comparison with *activated carbon*: From top left: Kinetic curves of sulfamethoxazole adsorption, top middle: Adsorption isotherms of sulfamethoxazole (C_e is equilibrium concertation and q_e is adsorbed amount per gram of adsorbent), top right: Adsorptive removal (%) of four different pollutants after 24 h when initial concentrations of the pollutants were 100 mg L^{-1}. Bottom row shows the structures of the tested pollutants.

Based on the literature, the adsorption capacity of **ActB** for sulfamethoxazole is higher than other porous materials such as modified *activated carbon*,[28] biochar,[29] or porous metal-organic framework (MOF) MIL-101.[30] Only a few metal-organic frameworks such as MOF-525 and MOF-545 with BET specific surface area exceeding 2000 m^2 g^{-1} exhibit higher adsorption capacity (ca. 600 mg g^{-1});[31] however, these zirconium MOFs display low stabilities in aqueous environments and are highly sensitive to pH.[32,33] **ActB** also exhibits higher adsorption capacity for diclofenac and tramadol than was observed on different carbon-based and biochar materials,[34,35] clays[36] or even MOFs.[37]

Physisorption of drugs can be potentially used not only for water purification, but also for drug delivery applications if the drug can be desorbed in physiological media. For this reason, we tested the desorption of sulfamethoxazole from **ActB** in pure water, methanol and phosphate saline buffer (PBS). To test these properties, the **ActB** was first fully loaded with sulfamethoxazole, separated and suspended in fresh water, methanol or PBS. In water we observed partial desorption ca. 25 % of adsorbed sulfamethoxazole, while >95% desorption was found in methanol and PBS all after 24 h at 25 °C.

As mentioned above, **ActB** can be prepared from readily available chemicals without any purification. To document the effect of air and moisture on its preparation, we prepared a batch named **ActB-wet** made from chemicals "as received" without any precaution against moisture or oxygen during the synthesis and subsequent workup. Additionally, a further batch named **ActB-semidry** was made from dry precursors under Ar atmosphere, however, the workup was done in an ambient atmosphere. Figure S1, S2 and Table S1, document the decrease in BET specific surface area, pore volume and adsorption capacities for sulfamethoxazole with increasing level of humidity **ActB** > **ActB-semidry** > **ActB-wet** (see also Figure S9 displaying adsorption isotherms of sulfamethoxazole). To highlight the potential of the newly discovered porous polymer, even **ActB-wet** still exhibit higher adsorption capacity of sulfamethoxazole than *activated carbon*.

Conclusions

In summary, we present the first member from the *Activated Borane* family of porous materials that, conveniently, can be readily prepared by simple heating from commercially available reagents. This new class of porous polymer has an unprecedented chemical nature and untapped structural variability. The presented data indicates that the application potential of *Activated Boranes* is not limited to the adsorption of pollutants but also of potential use in drug delivery and, indeed, we believe that many other applications will appear in the future.

Acknowledgement

References

[1] P. Van Der Voort, K. Leus, E. De Canck, Introduction to Porous Materials, Wiley-VCH Verlag GmbH & Co. KGaA, 2020

[2] F. Çeçen, Ö. Aktaş, Activated Carbon for Water and Wastewater Treatment, Wiley-VCH Verlag GmbH & Co. KGaA, 2011.

[3] L. Tan, B. Tan, *Chem. Soc. Rev.* **2017**, *46*, 3322–3356. https://doi.org/10.1039/C6CS00851H

[4] K. Geng, T. He, R. Liu, S. Dalapati, K. T. Tan, Z. Li, S. Tao, Y. Gong, Q. Jiang, D. Jiang, *Chem. Rev.* **2020**, *120*, 8814–8933. https://doi.org/10.1021/acs.chemrev.9b00550

[5] N. B. McKeown, *Polymer* **2020**, *202*, 122736. https://doi.org/10.1016/j.polymer.2020.122736

[6] J. García-Martínez, K. Li, Eds., Mesoporous Zeolites, Wiley-VCH Verlag GmbH & Co. KGaA, 2015.

[7] H. O. Pastore, S. Coluccia, L. Marchese, *Annu. Rev. Mater. Res.* **2005**, *35*, 351–395. https://doi.org/10.1146/annurev.matsci.35.103103.120732

[8] D. Zhao, Y. Wan, W. Zhou, Ordered Mesoporous Materials, Wiley-VCH Verlag GmbH & Co. KGaA, 2013.

[9] W. Zhang, Y. Tian, H. He, L. Xu, W. Li, D. Zhao, *National Science Review* **2020**, *7*, 1702–1725. https://doi.org/10.1093/nsr/nwaa021

[10] O. M. Yaghi, M. J. Kalmutzki, C. S. Diercks, Introduction to Reticular Chemistry: Metal-Organic Frameworks and Covalent Organic Frameworks, Wiley-VCH Verlag GmbH & Co. KGaA, 2019

[11] A. N. Alexandrova, A. I. Boldyrev, H.-J. Zhai, L.-S. Wang, Coord. Chem. Rev. **2006**, *250*, 2811–2866. https://doi.org/10.1016/j.ccr.2006.03.032

[12] D. Olid, R. Núñez, C. Viñas, F. Teixidor, *Chem. Soc. Rev.* **2013**, *42*, 3318. https://doi.org/10.1039/C2CS35441A

[13] D. Hnyk, M. McKee, Eds., Boron, The Fifth Element, Springer International Publishing, 2015. https://doi.org/10.1007/978-3-319-22282-0

[14] E. Hey-Hawkins, C. Viñas Teixidor, Eds., Boron-Based Compounds: Potential and Emerging Applications in Medicine, Wiley-VCH Verlag GmbH & Co. KGaA, 2018.

[15] L. Cerdán, A. Francés-Monerris, D. Roca-Sanjuán, J. Bould, J. Dolanský, M. Fuciman, M. G. S. Londesborough, *J. Mater. Chem. C* **2020**, *8*, 12806–12818. https://doi.org/10.1039/D0TC02309D

[16] L. Cerdán, J. Braborec, I. Garcia-Moreno, A. Costela, M. G. S. Londesborough, *Nat. Commun.* 2015, 6, 5958. https://doi.org/10.1038/ncomms6958

[17] D. F. Gaines, C. K. Nelson, J. C. Kunz, J. H. Morris, D. Reed, *Inorg. Chem.* **1984**, *23*, 3252–3254. https://doi.org/10.1021/ic00188a044

[18] J. W. E. Weiss, D. L. Bryce, *J. Phys. Chem. A* **2010**, *114*, 5119–5131. https://doi.org/10.1021/jp101416k

[19] J. Brus, J. Czernek, M. Urbanova, L. Kobera, A. Jegorov, *Phys. Chem. Chem. Phys.* **2017**, *19*, 487–495. https://doi.org/10.1039/C6CP06555D

[20] T. Harazono, Y. Hiroyama, T. Watanabe, *BCSJ* **1996**, *69*, 2419–2423.

[21] F. Mauri, N. Vast, C. J. Pickard, *Phys. Rev. Lett.* **2001**, *87*, 085506 (DOI: 10.1103/PhysRevLett.87.085506)

[22] M. Diaz, J. Jaballas, J. Arias, H. Lee, T. Onak, *J. Am. Chem. Soc.* **1996***, 118,* 4405–4410. https://doi.org/10.1021/ja954089y

[23] K. E. Murray, S. M. Thomas, A. A. Bodour, *Environ. Pollut.* **2010**, *158*, 3462–3471. https://doi.org/10.1016/j.envpol.2010.08.009

[24] M. Gavrilescu, K. Demnerová, J. Aamand, S. Agathos, F. Fava, *N. Biotechnol.* **2015**, *32*, 147–156. https://doi.org/10.1016/j.nbt.2014.01.001

[25] M. Valdez-Carrillo, L. Abrell, J. Ramírez-Hernández, J. A. Reyes-López, C. Carreón-Diazconti, *Environ. Sci. Pollut. Res.* **2020**, *27*, 44863–44891. https://doi.org/10.1007/s11356-020-10842-9

[26] Commission, E. Communication from the Commission to the European Parliament, the Council, and the European Economic 580 and Social Committee: European Union Strategic Approach to Pharmaceuticals in the Environment. EU Commision 2019, 128, 581, 13. https://ec.europa.eu/environment/water/water-dangersub/pdf/strategic_approach_pharmaceuticals_env.PDF

[27] L. Patrolecco, J. Rauseo, N. Ademollo, P. Grenni, M. Cardoni, C. Levantesi, M. L. Luprano, A. B. Caracciolo, *Sci. Total Environ.* **2018**, *640–641*, 1438–1446. https://doi.org/10.1016/j.scitotenv.2018.06.025

[28] Y. Liu, X. Liu, G. Zhang, T. Ma, T. Du, Y. Yang, S. Lu, W. Wang, *Colloid Surf. A-Physicochem. Eng. Asp.* **2019**, *564*, 131–141. https://doi.org/10.1016/j.colsurfa.2018.12.041

[29] F. Reguyal, A. K. Sarmah, *Sci. Total Environ.* **2018**, *628–629*, 722–730. https://doi.org/10.1016/j.scitotenv.2018.01.323

[30] X. Huang, Q. Hu, L. Gao, Q. Hao, P. Wang, D. Qin, *RSC Adv.* **2018**, *8*, 27623–27630. https://doi.org/10.1039/C8RA04789H

[31] K. Yu, I. Ahmed, D.-I. Won, W. I. Lee, W.-S. Ahn, *Chemosphere* **2020**, *250*, 126133. https://doi.org/10.1016/j.chemosphere.2020.126133

[32] D. Bůžek, J. Demel, K. Lang, *Inorg. Chem.* **2018**, *57*, 14290–14297. https://doi.org/10.1021/acs.inorgchem.8b02360

[33] D. Bůžek, S. Adamec, K. Lang, J. Demel: Metal-organic frameworks vs. buffers: Case study of UiO-66 stability, *Inorg. Chem. Front.* **2021**, *8*, 720-734. https://doi.org/10.1039/D0QI00973C

[34] A. O. Abo El Naga, M. El Saied, S. A. Shaban, F. Y. El Kady, *J. Mol. Liq.* **2019**, *285*, 9–19. https://doi.org/10.1016/j.molliq.2019.04.062

[35] L. Lonappan, T. Rouissi, S. Kaur Brar, M. Verma, R. Y. Surampalli, *Bioresour. Technol.* **2018**, *249*, 386–394. https://doi.org/10.1016/j.biortech.2017.10.039

[36] T. Thiebault, R. Guégan, M. Boussafir, *J. Colloid Interface Sci.* **2015**, *453*, 1–8. https://doi.org/10.1016/j.jcis.2015.04.029

[37] Z. Hasan, N. A. Khan, S. H. Jhung, *Chem. Eng. J.* **2016**, *284*, 1406–1413. https://doi.org/10.1016/j.cej.2015.08.087